Chapter 6

The transfer function approach

The analysis presented in chapters 3 and 4 illustrated how the signal from the reflectance and magneto-optic scanning microscopes can be expressed in a transfer function form, where the properties of the optical system are distinct from the properties of the sample. It was illustrated that the signal, from all the detection strategies discussed, can be expressed in the same characteristic form, as given by eq. (3.32), i.e.

$$I(x_s, y_s) = \iint_{-\infty}^{\infty} C(n_x, n_y; n_x', n_y')\, M(n_x, n_y; n_x', n_y') \cdot \exp\left\{2p\, j\left[(n_x - n_x')x_s + (n_y - n_y')y_s\right]\right\}\, dn_x\, dn_y\, dn_x'\, dn_y' \tag{3.32}$$

where the function $C(n_x, n_y; n_x', n_y')$ is the partially coherent transfer function, PCTF, and $M(n_x, n_y; n_x', n_y')$ is the medium function. The form of the PCTF depends upon whether the detection system is Type 1, where the PCTF is given by eq. (3.38), i.e.

$$C(n_x, n_y; n_x', n_y') = \iint_{-\infty}^{\infty} p_1(x + n_x\, l\, f, y + n_y\, l\, f)\, p_1{}^*(x + n_x'\, l\, f, y + n_y'\, l\, f) \cdot \left|p_2(x, y)\right|^2\, dx\, dy \tag{3.38}$$

or confocal, where the PCTF is given by eq. (3.73), i.e.

$$C(n_x, n_y; n_x', n_y') = \iint_{-\infty}^{\infty} \iint_{-\infty}^{\infty} p_1(x + n_x\, lf, y + n_y\, lf)\, p_1{}^*(x' + n_x'\, lf, y' + n_y'\, lf) \cdot p_c(x, y)\, p_c{}^*(x', y')\, G(x - x', y - y')\, dx dy dx'\, dy' \tag{3.73}$$

where the symbols have their usual meaning. The form of the medium function depends upon whether the detection technique is reflectance, where it is given by eq. (3.33), i.e.

$$M(n_x, n_y; n_x', n_y') = \Gamma(n_x, n_y)\, \Gamma^*(n_x', n_y') \tag{3.33}$$

single detector MO, where it is given by eq. (4.15), i.e.

$$M\left(n_x,n_y;n_x',n_y'\right)=\left(\Gamma^*\left(n_x',n_y'\right)\cos b+\Lambda^*\left(n_x',n_y'\right)\sin b\right)\cdot\left(\Gamma\left(n_x,n_y\right)\cos b+\Lambda\left(n_x,n_y\right)\sin b\right) \tag{4.15}$$

or differential detector MO, where it is given by eq. (4.42), i.e.

$$M\left(n_x,n_y;n_x',n_y'\right)=\left(\Gamma\left(n_x,n_y\right)\Gamma^*\left(n_x',n_y'\right)-\Lambda\left(n_x,n_y\right)\Lambda^*\left(n_x',n_y'\right)\right)\cos 4q+\left(\Gamma\left(n_x,n_y\right)\Lambda^*\left(n_x,n_y\right)+\Gamma^*\left(n_x',n_y'\right)\Lambda\left(n_x,n_y\right)\right)\sin 4q \tag{4.42}$$

where all symbols have their usual meaning. Hence, it can be seen that the same computational procedure can be adopted to model all the detection techniques discussed, where the PCTFs and medium functions are used interchangeably depending upon the scanning microscope configuration being investigated.

In the following chapter the transfer function approach is used to model the response of the detection strategies discussed previously, and illustrates the usefulness of the transfer function approach for comparing the imaging characteristics of scanning microscopes.

6.1 Calculation of the partially coherent transfer function

The following section describes how to generate the Type 1 and confocal PCTFs by the application of eq. (3.38) and eq. (3.73) respectively in computer code.

6.1.1 Generation of the Type 1 PCTF

Comparing eq. (3.38) with eq. (3.22) it can be seen that the process for generating the Type 1 PCTF is similar to that used for generating the incoherent OTF. However, the generation of the Type 1 PCTF is somewhat more complicated, in so much that the convolution process is a function of the objective aperture pupil function, its complex conjugate and the square magnitude of the collector aperture pupil function. Assuming clear, aberration free, circular apertures of equal diameter, under uniform incident illumination, for a particular set of spatial frequencies n_x, n_y, n_x' and n_y', the Type 1 PCTF is represented by the area of overlap between three circles representing

p_1 centred on $(n_x lf, n_y lf)$ and p_1* centred on $(n_x' lf, n_y' lf)$ which also falls within the circle defined by $|p_2|^2$ centred on $(0,0)$, and is illustrated in Fig. (6.1) [4,5,7,20,34,46].

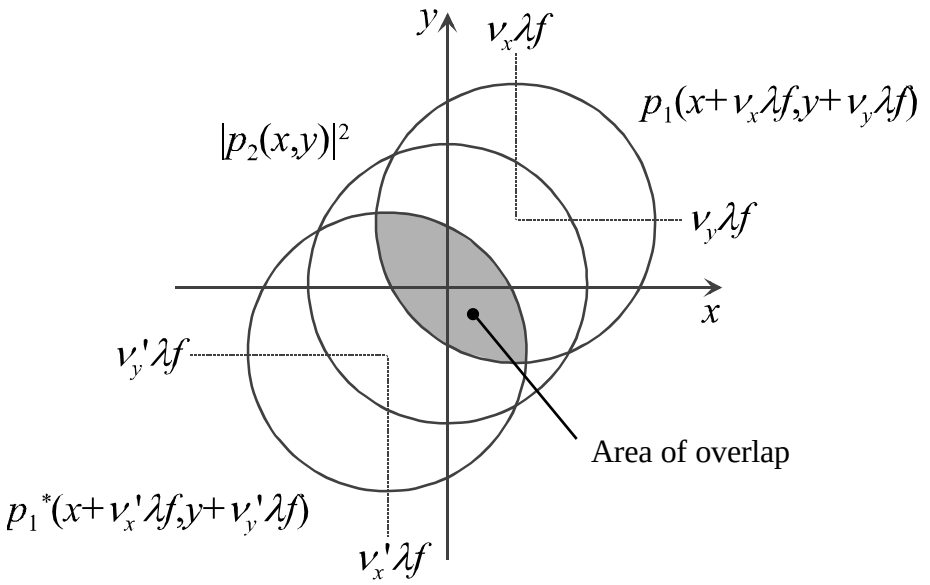

Figure 6.1 : *Generation of the Type 1 PCTF by the calculation of the area of overlap of the objective aperture pupil function, its complex conjugate, and the square magnitude of the collector aperture pupil function.*

The general form of the PCTF is a four dimensional function (of n_x, n_y, n_x', n_y'). Due to the complexities of generating a four dimensional transfer function, the PCTF is often restricted to imaging objects which are a function of a single direction. In which case the analysis is simplified significantly, and the Type 1 PCTF is reduced to a function of two variables, i.e.

$$C(n_x; n_x') = \iint_{-\infty}^{\infty} p_1(x + n_x l f, y)\, p_1^*(x + n_x' l f, y) \cdot |p_2(x, y)|^2 \, dx\, dy \quad . \tag{6.1}$$

Assuming clear, aberration free, circular apertures of equal diameter under uniform illumination, for a particular pair of spatial frequencies n_x and n_x', the PCTF is now represented by the area of overlap between three circles representing p_1 centred on $(n_x lf, 0)$ and p_1* centred on $(0, n_x' lf)$ that also falls within the circle defined by $|p_2|^2$ centred on $(0,0)$, and is illustrated in Fig. (6.2).

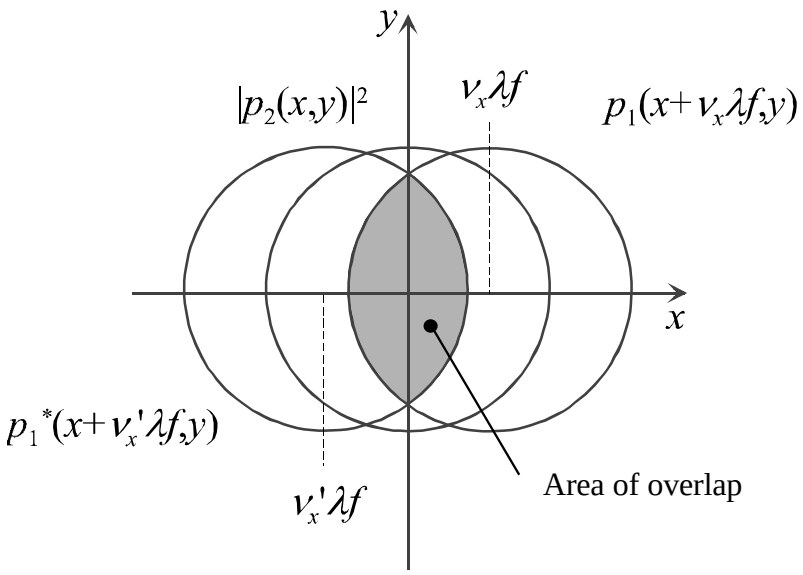

Figure 6.2 : *Generation of the Type 1 PCTF by the calculation of the area of overlap of the objective aperture pupil function, its complex conjugate, and the square magnitude of the collector aperture pupil function, when imaging in a single direction, i.e. x.*

The Type 1 PCTF algorithm

The following algorithm, written in pseudocode (see Appendix B), illustrates the computational procedure for calculating the Type 1 PCTF (for a one-dimensional object) following eq. (6.1) and Fig. (6.2).

Step 1 Input data
Matrix containing the objective aperture pupil function, p_o, which is of dimensions *adim* × *adim*.
Matrix containing the complex conjugate of the objective aperture pupil function, p_o*, which is of dimensions *adim* × *adim*.
Matrix containing the collector aperture pupil function, p_c, which is of dimensions *adim* × *adim*.
Temporary matrix, *temp*, of dimensions *adim* × (3∗*adim*), used during the convolution process.

Output data
Matrix containing the Type 1 PCTF which is of dimensions *tdim* × *tdim*, where *tdim* = (*2*×*adim*)+*1*.

Step 2 FOR *h = 0…*(*2*×*adim*) DO *Step 3* to *Step 7.* [#1]
Step 3 FOR *g = 0…*(*2*×*adim*) DO *Step 4* to *Step 7.* [#2]

Step 4

FOR $y = 1 \ldots adim$
  FOR $x = 1 \ldots adim$
    Set $temp(y, x + adim) = |p_c(y, x)|^2$ [#3];
    Set $temp(y, x) = 0$ [#4];
    Set $temp(y, x) = 0$ [#4];
  END;
END.

Step 5

FOR $y = 1 \ldots adim$
  FOR $x = 1 \ldots adim$
    Set $temp(y, x + g) = temp(y, x + g) \times p_o(y, x)$; [#5]
  END;
END;
FOR $y = 1 \ldots adim$
  FOR $x = 1 \ldots g$
    Set $temp(y, x) = 0$ [#4];
  END;
END;
FOR $y = 1 \ldots adim$
  FOR $x = (g + adim) \ldots (3 \times \text{adim})$
    Set $temp(y, x) = 0$ [#4];
  END;
END.

Step 6

FOR $y = 1 \ldots adim$
  FOR $x = 1 \ldots adim$
    Set $temp(y, x + h) = temp(y, x + h) \times p_o^*(y, x)$; [#6]
  END;
END;
FOR $y = 1 \ldots adim$
  FOR $x = 1 \ldots h$
    Set $temp(y, x) = 0$ [#4];
  END;
END;
FOR $y = 1 \ldots adim$
  FOR $x = (h + adim) \ldots (3 \times \text{adim})$
    Set $temp(y, x) = 0$ [#4];
  END;
END.

Step 7

Set $C(h, g) = \sum_{y=1}^{y=adim} \sum_{x=1}^{x=tdim} temp(y, x)$;

  END;
END;
STOP.

[#1] $h = 0$ corresponds to a displacement of the complex conjugate of the objective aperture pupil function by $n_x' lf = -adim$, and $h = 2 \times adim$ corresponds to $n_x lf = +adim$.

#2 $g = 0$ corresponds to a displacement of the objective aperture pupil function by, $n_x lf = -adim$ and $g = 2 \times adim$ corresponds to $n_x' lf = +adim$.
#3 Centre $|p_c|^2$ inside the *temp* matrix.
#4 Areas which do not overlap are set to zero.
#5 Multiply the matrix *temp*, by the objective aperture pupil function displaced by g - $n_x lf$.
#6 Multiply the matrix *temp*, by the complex conjugate of the objective aperture pupil function displaced by h - $n_x lf$.

It should be noted that the algorithm illustrated above is not optimised for speed of execution or memory usage, and only illustrates the general convolution process.

The Type 1 PCTF

Figure 6.3 illustrates the Type 1 PCTF for clear, aberration free, circular apertures of equal diameter under uniform incident illumination, generated using the algorithm described above.

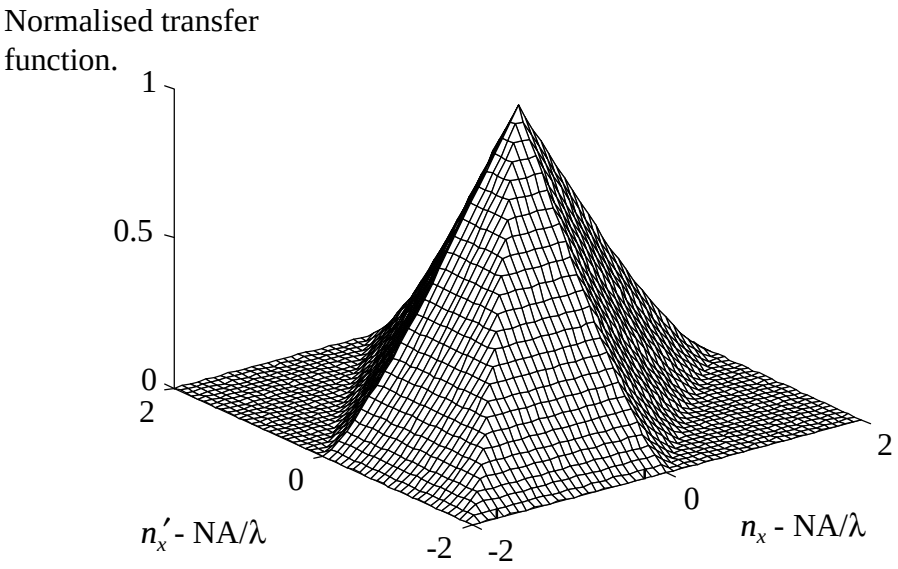

Figure 6.3 : *The Type 1 PCTF for clear, aberration free, circular apertures of equal diameter under uniform incident illumination.*

It should be noted that although n_x and n_x' are plotted in orthogonal directions, they do in fact represent spatial frequencies in the same direction, *x*.

Figure 6.4 illustrates the Type 1 PCTF for clear, aberration free, circular apertures of equal diameter under Gaussian ($w_{e^{-2}} = a/2$) incident illumination.

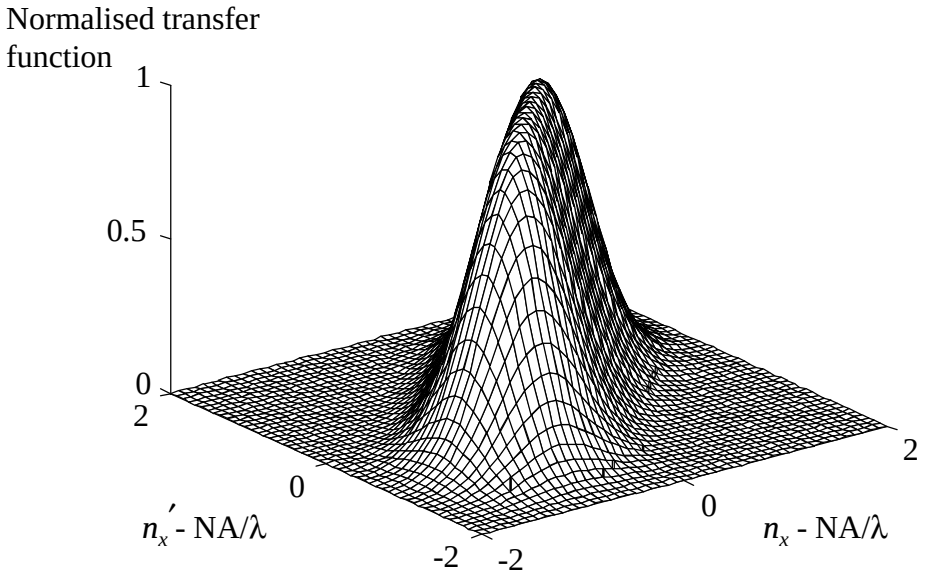

Figure 6.4 : *The Type 1 PCTF, for clear, aberration free, circular apertures of equal diameter under Gaussian incident illumination ($w_{e^{-2}} = a/2$).*

The partially coherent transfer function has a characteristic cut-off of $2NA/l$, which corresponds to the resolution limit of the imaging system. Figures 6.3 and 6.4 illustrate that, as seen previously in Fig. 5.3, the form of the incident illumination affects the shape of the Type 1 PCTF and hence, the imaging characteristics of the Type 1 scanning microscope.

Under uniform illumination the spatial frequency response of the Type 1 system is approximately linear with change in spatial frequency. However, under Gaussian illumination the high spatial frequency components are attenuated and the low frequency components are boosted, much like for the incoherent system described previously in sec. 3.1.2.

6.1.2 Generation of the confocal PCTF

When imaging objects which are restricted to detail in a single direction only, i.e. *x*, the confocal PCTF reduces to

$$C(n_x;n_x') = \iint\limits_{-\infty}^{\infty}\iint p_1(x+n_x\,lf,y)\,p_1{}^*(x'+n_x'\,lf,y') \cdot p_c(x,y)\,p_c{}^*(x',y')\,G(x-x',y-y')\,dx\,dy\,dx'\,dy' \tag{6.2}$$

where the symbols have their usual meaning. The generation of the confocal PCTF is a somewhat more complicated procedure compared with the Type 1 PCTF, and involves a convolution process which is a function of four variables.

The confocal PCTF algorithm

The following algorithm, written in pseudocode (see Appendix B), illustrates the computational procedure for calculating the confocal PCTF (for a one-dimensional object) following eq. (6.2).

Step 1 Input data
Matrix containing the objective aperture pupil function, p_o, which is of dimensions *adim* × *adim*.
Matrix containing the complex conjugate of the objective aperture pupil function, p_o*, which is of dimensions *adim* × *adim*.
Matrix containing the collector aperture pupil function, p_c, which is of dimensions *adim* × *adim*.
Matrix containing the complex conjugate of the collector aperture pupil function, p_c,* which is of dimensions *adim* × *adim*.
Matrix containing the FFT of the pinhole aperture pupil function, *G*, which is of dimensions *tdim* × *tdim*.
Temporary matrices, *temp1* and *temp2*, of dimensions *adim* × (*3*×*adim*), used during the convolution process.

Output data
Matrix containing the confocal PCTF which is of dimensions *tdim* × *tdim*, where *tdim* = (*2*×*adim*)-*3*.

Step 2 FOR *h = 0*…(2×*adim*) DO *Step 3* to *Step 11*. #1
Step 3 FOR *g = 0* …(2×*adim*) DO *Step 4* to *Step 11*. #2
Step 4 FOR *y = 1*…*adim* DO
FOR *x = 1*… *adim* DO
Set *temp1*(*y*, *x*+*adim*) = p_c(*y*, *x*); #3
Set *temp1*(*n*, *m*) = *0*; #4
Set *temp1*(*n*, *m*+*2*×*adim*) = *0*; #4

END;
END.

Step 5 FOR $y = 1 \ldots adim$ DO *Step 6* to *Step 9*.

Step 6 FOR $x = 1 \ldots adim$ DO *Step 7* to *Step 9*.

Step 7 FOR $n = 1 \ldots adim$

FOR $m = 1 \ldots adim$

Set $temp2(n, m+adim) = p_c^*(n, m) \times G(y - n, x - m)$; #5

Set $temp2(n, m) = 0$; #4

Set $temp2(n, m+2 \times adim) = 0$; #4

END;

END.

Step 8 FOR $n = 1 \ldots adim$

FOR $m = 1 \ldots adim$

Set $temp2(n, m+h) = temp2(n, m+h) \times p_o^*(n, m)$; #6

END;

END;

FOR $n = 1 \ldots adim$

FOR $m = 1 \ldots h$

Set $temp2(n, m) = 0$; #4

END;

END;

FOR $n = 1 \ldots adim$

FOR $m = (h+adim) \ldots (3 \times adim)$

Set $temp2(n, m) = 0$; #4

END;

END.

Step 9 Set $temp1(y+adim, x+adim) = temp1(y+adim, x+adim) \times \sum_{n=1}^{n=adim} \sum_{m=1}^{m=tdim} temp2(n,m)$; #7

END;

END.

Step 10 FOR $y = 1 \ldots adim$

FOR $x = 1 \ldots adim$

Set $temp1(y, x+g) = temp1(y, x+g) \times p_o(y, x+g)$; #8

END;

END;

FOR $y = 1 \ldots adim$

FOR $x = 1 \ldots h$

Set $temp1(y, x) = 0$; #4

END;

END;

FOR $y = 1 \ldots adim$

FOR $y = (g+adim) \ldots (3 \times adim)$

Set $temp1(y, x) = 0$; #4

END;

END.

Step 11

Set $C(h, g) = \sum_{y=1}^{y=adim} \sum_{x=1}^{x=tdim} temp1(y, x)$;

END;
END;
STOP.

[#1] $h = 0$ corresponds to a displacement of the complex conjugate of the objective aperture pupil function by $n_x' lf = -adim$, and $h = 2 \times adim$ corresponds to $n_x lf = +adim$.
[#2] $g = 0$ corresponds to a displacement of the objective aperture pupil function by, $n_x lf = -adim$ and $g = 2 \times adim$ corresponds to $n_x' lf = +adim$.
[#3] Centre p_c inside the *temp1* matrix.
[#4] Areas which do not overlap are set to zero.
[#5] Centre p_c* inside the *temp2* matrix, multiplied by the shifted FFT of the pinhole aperture pupil function.
[#6] Multiply the matrix *temp2,* by the complex conjugate of the objective aperture pupil function displaced by $h - \nu_x' \lambda f$.
[#7] Sum the matrix *temp2* over all {*m, n*} space.
[#8] Multiply the matrix *temp1*, by the objective aperture pupil function displaced by $g - n_x lf$.

It should be noted that the algorithm above is not optimised for speed of execution or memory usage and only illustrates the general convolution process.

The confocal PCTF

Figure 6.5 illustrates the confocal PCTF for clear, aberration free, circular apertures of equal diameter under uniform incident illumination, employing an infinitesimally small pinhole (ideal confocal), generated using the algorithm described above.

Figure 6.6 illustrates the confocal PCTF for clear, aberration free, circular apertures of equal diameter under uniform incident illumination, employing a finite sized pinhole of radius $0.75 l/NA$.

Comparing Fig. 6.5 with Fig 6.3 illustrates that the ideal confocal PCTF is very different in shape to the Type 1 PCTF. As the size of the confocal pinhole increases, then the shape of the confocal PCTF changes and the confocal PCTF begins to resemble the Type 1 PCTF. Such a result was illustrated in sec. 3.3 where the analysis

indicated that the expression representing the signal from the confocal reflectance scanning microscope reverted to that of the Type 1 system for large pinhole sizes.

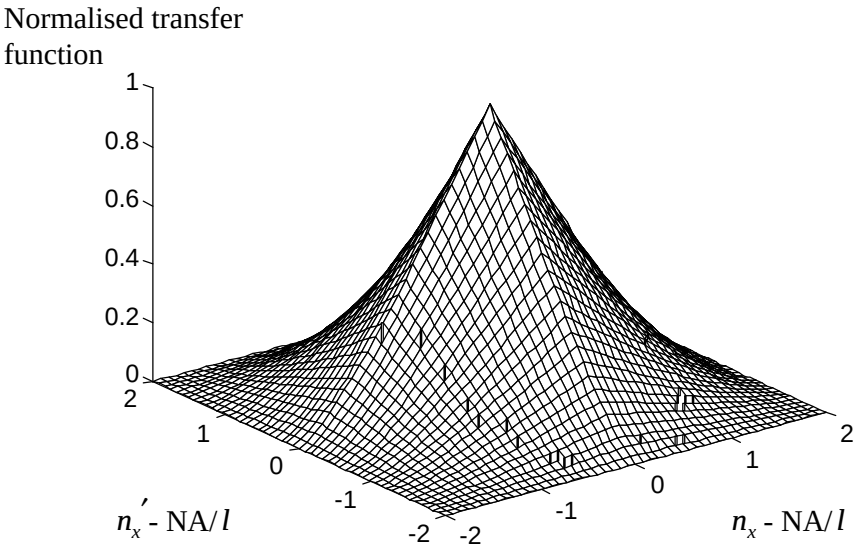

Figure 6.5 : *The ideal confocal PCTF, for clear, aberration free, circular apertures under uniform incident illumination, generated using the confocal PCTF algorithm.*

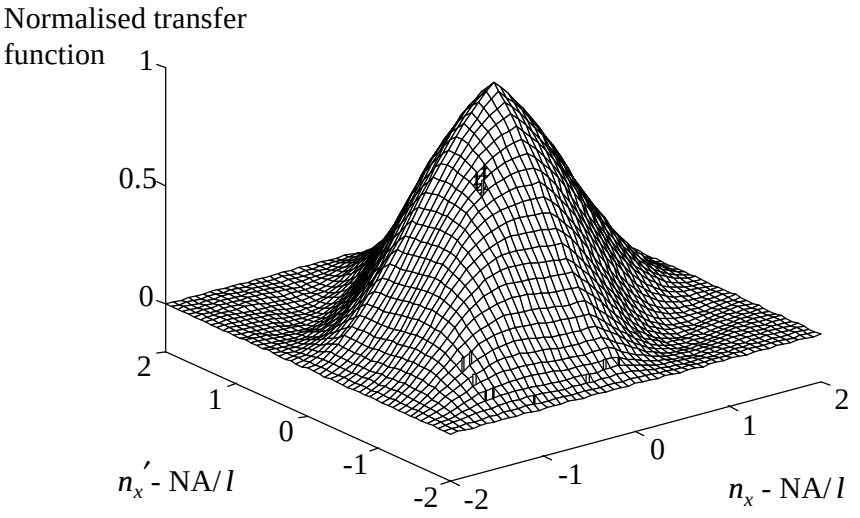

Figure 6.6 : *The confocal PCTF for a finite sized pinhole, of radius 0.75l/NA, for clear aberration free, circular apertures of equal diameter under uniform incident illumination.*

6.2 Modelling the ordinary reflectance scanning microscope

In this section the imaging process in the reflectance scanning microscope is discussed using the transfer function approach. The signal from the reflectance scanning microscope can be expressed in the characteristic form of eq. (3.32) where the PCTF depends upon whether the detection channel is Type 1 or confocal, and the medium function is given by eq. (3.33). Considering objects which contain information in a single direction only, *x*, then the medium function may be recast in the simplified form

$$M(n_x; n_x') = \Gamma(n_x)\Gamma^*(n_x') \tag{6.3}$$

and the characteristic equation, eq. (3.32) reduces to the form

$$I(x_s) = \iint_{-\infty}^{\infty} \left[C(n_x; n_x')\, M(n_x; n_x') \exp\{2pjn_x x_s\} dn_x \right] \exp\{-2p\, jn_x' x_s'\}\ dn_x' \Big|_{x_s' = x_s} \tag{6.4}$$

where the PCTF is generated using the analysis presented in the previous section. Eq. (6.4) illustrates that the response of the Type 1 reflectance scanning microscope to a simple one-dimensional object can be generated very easily using Fourier transform techniques.

6.2.1 The Type 1 system

The computational procedure for generating the Type 1 PCTF has been described in detail in sec. 6.1. The cut-off spatial frequency of the matrix representing the PCTF governs the resolution of the output signal. Using the properties of the discrete Fourier transform [42], the spatial resolution, Δx, is given by

$$\Delta x = \frac{1}{(2n_c)} \tag{6.5}$$

where n_c is the cut-off spatial frequency of the PCTF matrix. If the cut-off remains at $2NA/l$, then the output resolution will be given by $0.25l/NA$. For a wavelength of 514nm and NA of 0.5 this gives an output resolution of 0.25μm. Hence, to improve the resolution of the output signal the PCTF matrix should be centred in a much larger matrix of size $mdim \times mdim$, where $mdim$ is a function of $tdim$ (the dimension of the

matrix representing the PCTF), i.e. $mdim = c \times tdim$, where c is a integer, such that the cut-off spatial frequency of the larger matrix is given by

$$n_c = \frac{2cNA}{l} \quad . \tag{6.6}$$

In which case, using the properties of the discrete Fourier transform, the output resolution is given by

$$\Delta x = \frac{1}{2n_c} = \frac{l}{4cNA} \quad . \tag{6.7}$$

For example, if the cut-off frequency of the larger matrix is $16NA/l$, i.e. c=8 and $mdim = 8 \times tdim$, then the resolution of the output signal will be $0.03125l/NA$, which corresponds to a resolution of 0.03μm for a wavelength of 514nm and an NA of 0.5.

Computational procedure

Figure 6.7 illustrates the signal generation process, using the transfer function approach, for the Type 1 reflectance system when imaging a simple one-dimensional object, and is described in detail as follows.

Step 1

- Generate a matrix containing the objective aperture pupil function, p_o, which is of dimensions $adim \times adim$.
- Generate a matrix containing the collector aperture pupil function, p_c, which is of dimensions $adim \times adim$.
- Generate a vector representing the reflectance characteristics of the sample, *r*, which is of length *mdim*.

The resolution of the sample vector depends upon the value of *mdim*, and is determined using the analysis described in the previous section.

Step 2 Generate the Type 1 PCTF which is contained in a matrix of dimensions $tdim \times tdim$, where $tdim = 2 \times adim$, using the computational procedure described in sec. 6.1.1.

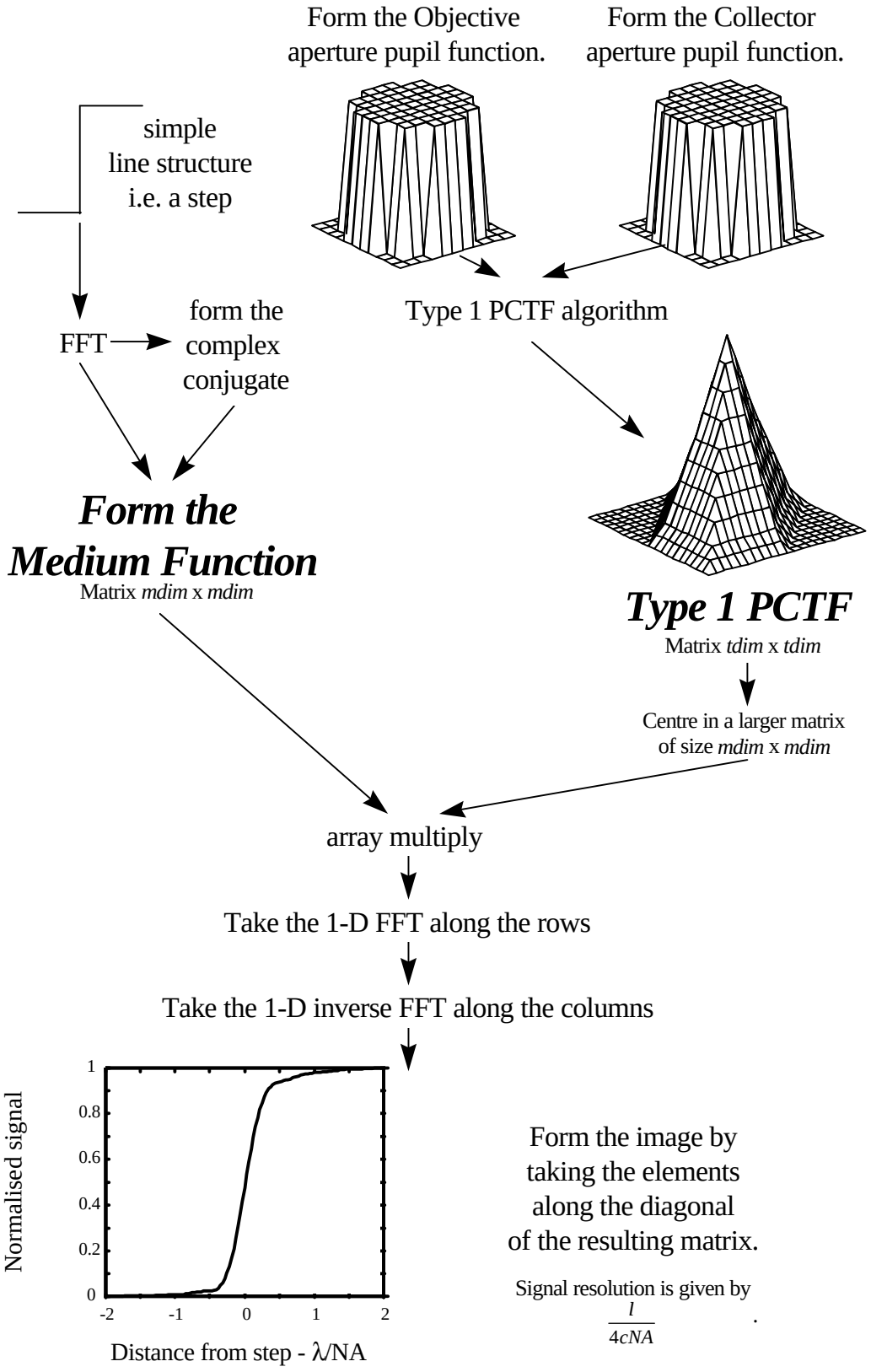

Figure 6.7 : *The signal generation process in the Type 1 reflectance scanning microscope, using the transfer function approach.*

Step 3 Centre the matrix containing the Type 1 PCTF inside a larger matrix, *P*, of dimensions $mdim \times mdim$, to give an output signal resolution of $l / 2cNA$.

Step 4 Generate a vector representing the samples spatial frequency spectrum, Γ, by taking the one-dimensional Fast Fourier Transform (FFT) of the vector *r*.

Step 5 Calculate a vector , Γ*, containing the complex conjugate of the vector Γ.

Step 6 Form a matrix, *M*, representing the medium function by copying the vector Γ, representing the sample spatial frequency spectrum into the rows of *M*, and array multiplying the columns by the vector, Γ*, representing the complex conjugate of the sample spatial frequency spectrum.

Step 7 Array multiply the matrix representing the *PCTF* , *P*, by the matrix representing the medium function, *M*.

Step 8 Take the FFT along the rows of the resulting matrix.

Step 9 Take the inverse FFT along the columns of the resulting matrix.

Step 10 The signal, *I*, which is an intensity signal, is calculated by forming a vector, of length *mdim*, containing the values along the diagonal of the resulting matrix, i.e. $(x_s = x_s')$.

The transfer function algorithm

The following algorithm, written in pseudocode (see Appendix B), illustrates the computational procedure for calculating the response of the Type 1 reflectance scanning microscope using the transfer function approach, when imaging simple one-dimensional objects.

Step 1 Input data. Matrix containing the objective aperture pupil function - p_o, of dimensions *adim* × *adim*
Matrix containing the collector aperture pupil function - p_c, of dimensions *adim* × *adim*
Vector containing the sample reflectance characteristics - *r*, of length *mdim* (one-dimensional reflectance object).
Matrix to contain the PCTF - *P*, of dimensions *mdim* × *mdim*.
Matrix to contain the medium function - *M*, of dimensions *mdim* × *mdim*.
Vector to contain the reflectance spectrum of the object - Γ, of length *mdim*.
Temporary vectors - *dummy* and *temp*, of length *mdim*.

Output data. Vector containing the signal from the scanning microscope - *I*, of length *mdim.*

Step 2 Generate a matrix representing the Type 1 PCTF, *PCTF*, using the algorithm presented in sec. 6.1, which is of dimensions *tdim* × *tdim*, where *tdim* = 2×*adim.*

Step 3
```
FOR y = 1…mdim
    FOR x = 1…mdim
        Set P(y, x) = 0;
    END;
END;
FOR y = 1…tdim
    FOR x = 1…tdim
        Set P(y + ((mdim-tdim)/2), x + ((mdim-tdim)/2)) =
                                        PCTF(y, x);#1
    END;
END.
```

Step 4 Set Γ = Fast Fourier Transform (*r*). #2

Step 5
```
FOR x = 1…mdim
    Set ℜ ( Γ*( x ) ) =  ℜ ( Γ( x ) ); #3
    Set ℑ ( Γ*( x ) ) =  - ℑ ( Γ( x ) );
END.
```

Step 6
```
FOR y = 1…mdim
    FOR x = 1…mdim
        Set M(y, x) = Γ( x );
    END;
END;
FOR y = 1…mdim
    FOR x = 1…mdim
        Set M(y, x) = M(y, x) × Γ*( y );
    END;
END.
```

Step 7
```
FOR y = 1…mdim
    FOR x = 1…mdim
        Set P(y, x) = P(y, x) × M(y, x);
```

```
            END;
        END.
Step 8  FOR y = 1…mdim
            FOR x = 1…mdim
                Set dummy(x ) = P(y, x);
            END;
            Set dummy = Fast Fourier Transform (dummy); #2
            FOR x = 1…mdim
                Set temp(y, x) = P(x );
            END;
        END.
Step 9  FOR y = 1…mdim
            FOR x = 1…mdim
                Set dummy(x ) = P(x, y);
            END;
            Set dummy = Inverse Fast Fourier Transform (dummy); #4
            FOR x = 1…mdim
                Set P(x, y) = dummy(x );
            END;
        END.
Step 10 FOR x = 1…mdim
            Set I (x ) = P(x, x);
        END;
        STOP.
```

#1 Centre the PCTF inside the larger *temp* matrix of dimensions $mdim \times mdim$.
#2 Fast Fourier Transform algorithm is described in reference 6.
#3 $\Re$ - represents the real component, $\Im$ - represents the imaginary component.
#4 Inverse Fast Fourier Transform algorithm is described in reference 6.

Step response

Figure 6.8 illustrates the step response of the Type 1 reflectance scanning microscope generated using the transfer function algorithm described above. The responses were generated using clear, aberration free, circular apertures of equal diameter, under uniform and Gaussian ($w_{e^{-2}} = a/2$) incident illumination. The responses illustrated in Fig. 6.8 have been generated using the Type 1 PCTFs illustrated in Fig. 6.3 and Fig. 6.4.

Comparison of Fig. 5.3 and Fig. 6.8 illustrates that the two approaches to modelling the imaging process in the Type 1 reflectance scanning microscope, the direct calculation and transfer function approaches, produce exactly the same results when

imaging simple one-dimensional objects. This gives great confidence in the validity and accuracy of both methods.

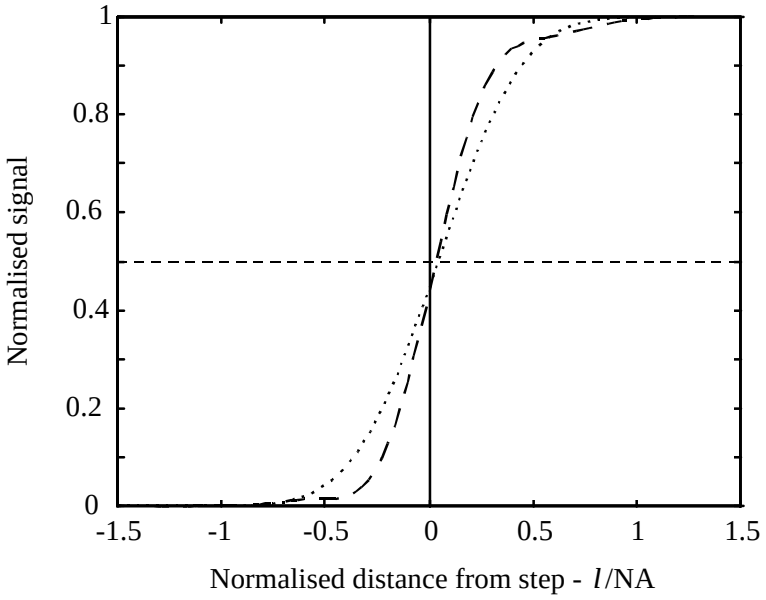

Figure 6.8 : *The step response of the Type 1 reflectance scanning microscope, for clear, aberration free, circular apertures under uniform (solid dashed line) and Gaussian ($w_{e^{-2}} = a/2$) (dotted line) incident illumination. Solid line represents the edge of the step.*

The disadvantage with the transfer function approach, is it is computationally demanding to produce two-dimensional images, due to the complexities of generating a four-dimensional transfer function. Hence, use of the transfer function approach in this thesis is limited to one-dimensional imaging only.

6.2.2 The confocal system

The computational procedure for calculating the response of the confocal reflectance scanning microscope, using the transfer function approach, follows directly from the algorithm described in detail in sec. 6.2.1. However, when calculating the response of the confocal configuration, the Type 1 PCTF should be replaced by the confocal PCTF, and then the same procedure for calculating the output signal can be applied. The computational procedure for generating the confocal PCTF has been described in detail in sec. 6.1. The procedure for increasing the resolution of the output signal in

the Type 1 system, described in sec 6.2.1 can be applied in the confocal case. Hence, the resolution of output signal from the confocal system can be increased by centring the confocal PCTF in a much larger matrix of dimensions $mdim \times mdim$, where $mdim$ is a function of $tdim$, i.e. $mdim = c \times tdim$, where c is a integer.

Step response

Figure 6.9 illustrates the step response of the confocal reflectance scanning microscope generated using the transfer function algorithm with the confocal PCTF. The response was generated using clear, aberration free, circular apertures of equal diameter, under uniform incident illumination, with an infinitesimally small confocal pinhole (ideal case). Also illustrated in Fig 6.9 is the step response of the Type 1 configuration under the same conditions.

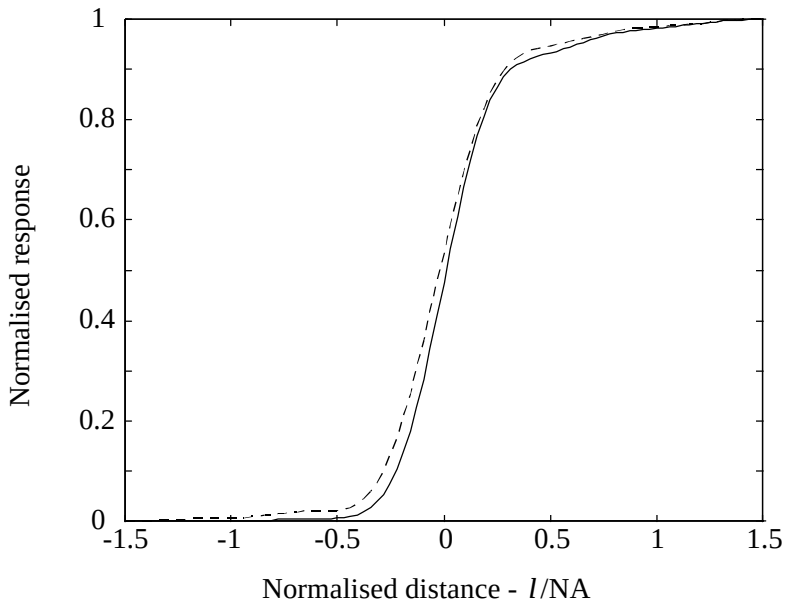

Figure 6.9 : *The step response of the ideal confocal reflectance scanning microscope, for clear, aberration free, circular apertures under uniform incident illumination, (solid line), and the step response of the Type 1 reflectance scanning microscope for the same conditions (dotted line).*

Figure 6.9 illustrates that the response of the confocal reflectance system is sharper as compared to the Type 1 system. This implies that the confocal system exhibits an improvement in resolution over the Type 1 case, as observed by other workers

[4,5,69,71,72,73]. The level of resolution improvement is perhaps illustrated more clearly by considering the impulse response.

Impulse response

Figure 6.10 illustrates the response of the confocal reflectance scanning microscope to a 1-D line of impulses (extending in the *y* direction). This is usually called the line spread function but here, since only 1-D objects are being dealt with, it will also be referred to as the impulse response. The response illustrated in Fig. 6.10 has been generated using clear, aberration free, circular apertures of equal diameter, under uniform incident illumination for the case of an ideal infinitesimally small pinhole, generated using the transfer function algorithm. Also illustrated is the corresponding impulse response of the Type 1 configuration, and the impulse response of the confocal system with a finite sized confocal pinhole.

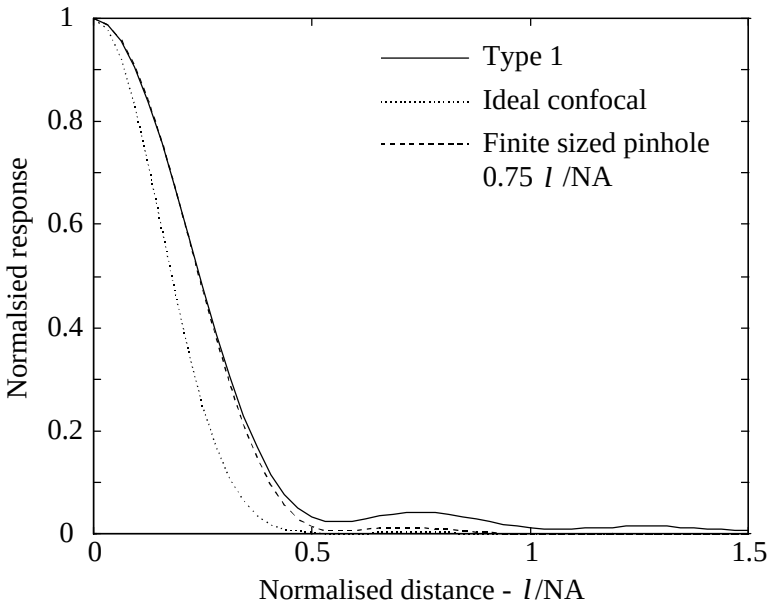

Figure 6.10 : *Plots of impulse response for the ideal confocal (dotted line), the confocal with finite sized pinhole (dashed line), and the Type 1 (solid line),reflectance scanning microscopes, for clear, aberration free, circular apertures of equal diameter under uniform incident illumination.*

Figure 6.10 clearly illustrates the resolution advantages of the confocal reflectance scanning microscope. The response of the confocal imaging system is narrower than that of the Type 1 optical system, which agrees with results produced by other researchers [4,5,53,70], and it is because of this that confocal systems are said to have improved lateral resolution. Another important observation is that the effect of the sidelobes due to the Airy disc focused spot is suppressed in the confocal case. It should be pointed out that the resolution improvement in the confocal optical system is not true super-resolution, since the confocal PCTF exhibits the same cut-off spatial frequency as the Type 1 optical system ($2NA/\lambda$). The effective improvement of the resolution of the confocal system can be explained by non-linear effects introduced at the optical detector, where diffraction orders are brought to interference in the detector plane, even when they do not overlap in the collector plane. However, as the size of the confocal pinhole increases these non-linear effects disappear [71].

6.2.3 Pinhole size and resolution issues in the confocal reflectance scanning microscope

It is instructive to investigate the effects which a finite sized pinhole has upon the resolution and imaging properties of the confocal reflectance scanning microscope. An infinitesimally small pinhole is an idealistic aperture which cannot be implemented in real systems. Hence, the optimum pinhole size must be chosen which will produce the best improvement in lateral resolution compared with the Type 1 configuration.

Figure 6.11 illustrates a plot of full width at half maximum (FWHM) of the impulse response of the confocal reflectance scanning microscope as a function of pinhole radius. The responses were generated using the transfer function approach described previously with clear, aberration free, circular apertures of equal diameter, under uniform illumination. Also shown is a plot of published data [53,72,73]. The agreement is good.

For a pinhole radius less than $0.75l$/NA, the impulse response begin to narrow, leading to improved lateral resolution. If the pinhole radius is greater than $1.5l$/NA then no significant resolution improvement is observed over the Type 1 configuration.

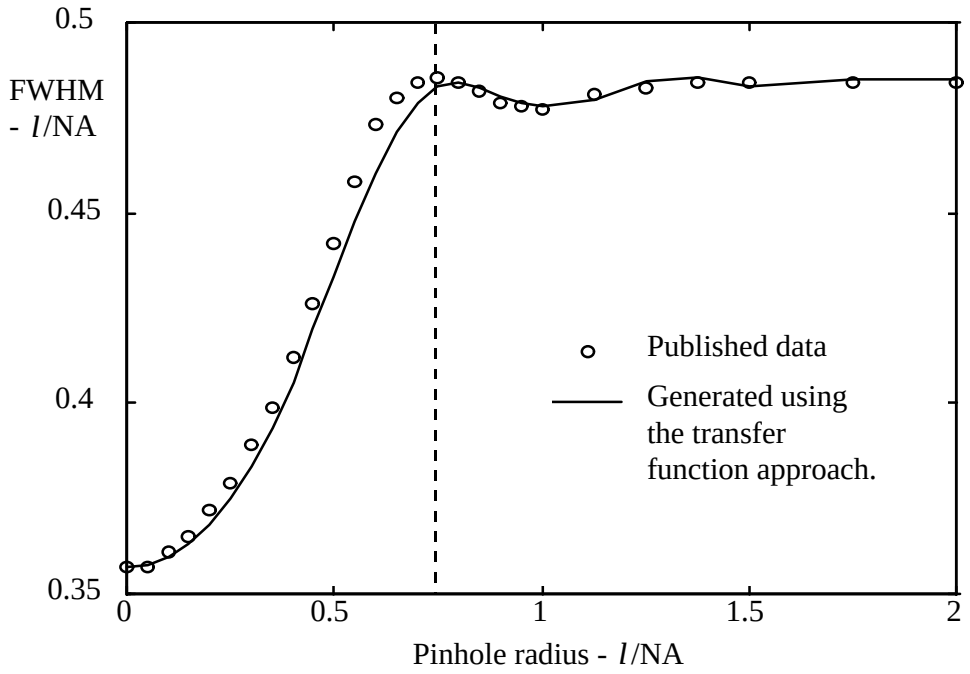

Figure 6.11 : *Plot of FWHM of the impulse response of the confocal reflectance scanning microscope as a function of pinhole size (solid line). Also illustrated is a plot of published data (circles).*

The optimum size of the pinhole depends largely on the wavelength of the illumination and the numerical aperture of the auxiliary lens. Results produced by Braat [71] illustrate that for a pinhole diameter less than 0.4λ/NA the signal from the confocal system is comparable with that of the ideal confocal system, and this agrees very well with the results outlined in Fig. 6.11. For a wavelength of 514nm, an auxiliary lens NA of 0.05 (realistic values) then the optimum pinhole diameter will be 10μm.

It should be noted that for very small pinhole radii the magnitude of the step response decreases rapidly since the reduced pinhole size restricts the amount light which reaches the photo-detector.

6.3 Modelling the single detector MO scanning microscope

In this section the imaging process in the single detector MO scanning microscope is discussed, using the transfer function approach. The signal from the single detector MO scanning microscope can be expressed in the characteristic form of eq. (3.32), where the PCTF depends upon whether the detection channel is Type 1 or confocal, and the medium function is given by eq. (4.15). Considering objects which contain information in a single direction only, *x*, then the medium function may be recast in the simplified form

$$M(n_x;n_x') = \left(\Gamma^*(n_x')\cos b + \Lambda^*(n_x')\sin b\right)\cdot\left(\Gamma(n_x)\cos b + \Lambda(n_x)\sin b\right) \quad (6.8)$$

and the characteristic equation, eq. (3.32), can be expressed in the form of eq. (6.4).

The following analysis is directed to calculating the form of the readout signal for both the Type 1 and confocal configurations, when imaging simple one-dimensional objects.

6.3.1 The Type 1 system

The computational procedure for calculating the response from the Type 1 single detector MO scanning microscope follows directly from the procedure described in sec. 6.2.1. However, the medium function in the single detector MO scanning microscope, eq. (6.8), is different to that of the reflectance scanning microscope. The computational procedure for calculating the Type 1 PCTF has been described in detail in sec. 6.1. The procedure for increasing the resolution of the output signal in the Type 1 reflectance scanning microscope, described in sec 6.2.1 can also be applied in the single detector MO system.

The transfer function algorithm

The algorithm for generating the response from the Type 1 single detector MO scanning microscope to a simple one-dimensional MO object is a modified version of that presented in sec. 6.2.1, and is illustrated below.

Step 1 Input data.

Matrix containing the objective aperture pupil function - p_o, of dimensions *adim* × *adim*

Matrix containing the collector aperture pupil function - p_c, of dimensions *adim* × *adim*

Vector containing the sample reflectance characteristics - *r*, of length *mdim* (one-dimensional MO object)

Vector containing the sample phase characteristics - f, of length *mdim* (one-dimensional MO object)

Vector containing the sample Kerr rotation characteristics - *k*, of length *mdim* (one-dimensional MO object)

The angle of the analyser transmission axis - b.

Matrix to contain the PCTF - *P*, of dimensions *mdim* × *mdim*.

Matrix to contain the medium function - *M*, of dimensions *mdim* × *mdim*.

Vector to contain the MO spectrum of the object - Λ, of length *mdim*.

Vector to contain the reflectance spectrum of the object - Γ, of length *mdim*.

Temporary vectors - *dummy* and *temp*, of length *mdim*.

Output data. Vector containing the signal from the scanning microscope - *I*, of length *mdim*.

Step 2 Generate a matrix representing the Type 1 PCTF, *PCTF*, using the algorithm presented in sec. 6.1, which is of dimensions *tdim* × *tdim*, where *tdim* = 2×*adim*.

Step 3

FOR *y = 1…mdim*
  FOR *x = 1…mdim*
    Set *P*(*y*, *x*) = 0;
  END;
END;
FOR *y = 1…tdim*
  FOR *x = 1…tdim*
    Set *P*(*y* + ((*mdim*-*tdim*)/2), *x* + ((*mdim*-*tdim*)/2)) = *PCTF*(*y*, *x*);[#1]
  END;
END.

Step 4

Set Γ = Fast Fourier Transform (*r*); [#2]
Set Λ = Fast Fourier Transform (*r* .× f .× *tan*(*k*)). [#3]

Step 5

FOR *x = 1…mdim*
  Set ℜ (Γ*(*x*)) = ℜ (Γ(*x*)); [#4]
  Set ℑ (Γ*(*x*)) = - ℑ (Γ(*x*));
END;
FOR *x = 1…mdim*
  Set ℜ (Λ*(*x*)) = ℜ (Λ(*x*)); [#4]
  Set ℑ (Λ*(*x*)) = - ℑ (Λ(*x*));
END.

Step 6 FOR $y = 1 \ldots mdim$
FOR $x = 1 \ldots mdim$
Set $M(y, x) = (\Gamma(x) cos b + \Lambda(x) sin b)$
$\times (\Gamma^*(y) cos b + \Lambda^*(y) sin b)$;
END;
END.

Step 7 FOR $y = 1 \ldots mdim$
FOR $x = 1 \ldots mdim$
Set $P(y, x) = P(y, x) \times M(y, x)$;
END;
END.

Step 8 FOR $y = 1 \ldots mdim$
FOR $x = 1 \ldots mdim$
Set $dummy(x) = P(y, x)$;
END;
Set *dummy* = Fast Fourier Transform (*dummy*); [#5]
FOR $x = 1 \ldots mdim$
Set $temp(y, x) = P(x)$;
END;
END.

Step 9 FOR $y = 1 \ldots mdim$
FOR $x = 1 \ldots mdim$
Set $dummy(x) = P(x, y)$;
END;
Set *dummy* = Inverse Fast Fourier Transform (*dummy*); [#4]
FOR $x = 1 \ldots mdim$
Set $P(x, y) = dummy(x)$;
END;
END.

Step 10 FOR $x = 1 \ldots mdim$
Set $I(x) = P(x, x)$;
END;
STOP.

[#1] Centre the PCTF inside the larger *temp* matrix of dimensions $mdim \times mdim$.
[#2] Fast Fourier Transform algorithm is described in reference 6.
[#3] $.\times$ indicates array multiplication.
[#4] $\Re$ - represents the real component, $\Im$ - represents the imaginary component.
[#5] Inverse Fast Fourier Transform algorithm is described in reference 6.

Step response

It is common to employ the single detector MO scanning microscope with the analyser transmission axis aligned at 8° to the extinction position [20], i.e. $b \approx 82°$, where the optimum signal-to-noise ratio is observed in the output signal. Figure 6.12

illustrates step responses of the single detector MO scanning microscope, generated using the transfer function algorithm, for analyser orientations of $b = 90°$ and $b = 82°$. The responses were generated using clear, aberration free, circular apertures of equal diameter, under uniform incident illumination, using a MO sample of uniform ordinary reflectance (r_x equal to unity) and zero phase.

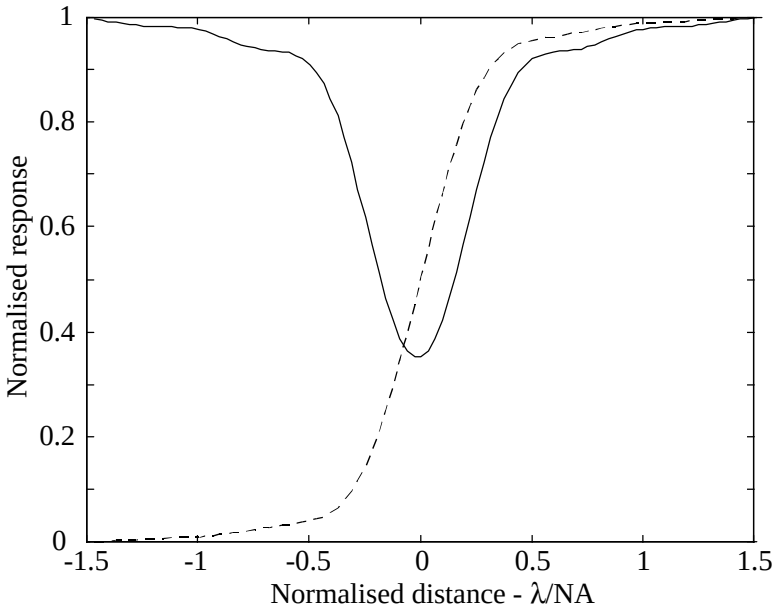

Figure 6.12 : *The step response of the Type 1 single detector MO scanning microscope for clear, aberration free, circular apertures of equal diameter under uniform incident illumination, for an analyser orientation of b=90°(solid line), and b=82° (dashed line) to the angle of incident polarisation.*

Again, comparison of Fig. 6.12 and Fig. 5.9 illustrates that the two approaches to modelling the imaging process in the Type 1 single detector MO scanning microscope, the direct calculation and transfer function approaches, produce exactly the same results when imaging simple one-dimensional objects.

An interesting result of Fig. 6.12 is that in the case of an analyser misalignment of 8°, the step response clearly follows the change in polarity of the step object, a result that is observed experimentally [20].

Impulse response

Figure 6.13 illustrates the impulse response of the Type 1 single detector MO system generated using the transfer function algorithm. The response was generated using clear, aberration free, circular apertures of equal diameter under uniform incident illumination, for a MO sample of uniform ordinary reflectance (equal to unity) and zero phase, with an analyser orientation of $b=90°$ (the extinction position). Also illustrated is the impulse response of the Type 1 reflectance system under the same conditions.

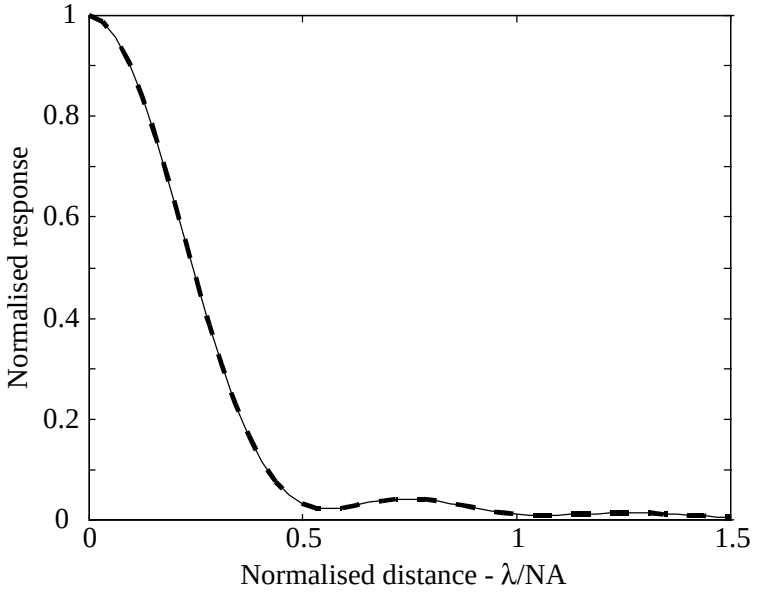

Figure 6.13 : *The impulse response of the Type 1 single detector MO scanning microscope for clear, aberration free, circular apertures of equal diameter under uniform incident illumination (solid line), for an analyser orientation of $b=90°$ to the angle of incident polarisation. Also illustrated is the impulse response of the Type 1 reflectance system (bold dashed line).*

An interesting result is that the impulse response on the Type 1 single detector MO system, i.e. the response for $\tan(a(x)) = d(x)$, is exactly the same as the impulse response of the Type 1 reflectance system for an object which is an impulse in reflectance, i.e. $r(x) = d(x)$. Hence, it can be deduced that the Type 1 single detector MO system exhibits imaging characteristics similar to that of the Type 1 reflectance

system described previously, providing the MO sample is of uniform ordinary reflectance and that the analyser is set to extinction.

6.3.2 The confocal system

The computational procedure, using the transfer function approach, for calculating the response of the confocal single detector MO scanning microscope follows directly from the algorithm described in detail in sec. 6.3.1. However, when calculating the response of the confocal configuration, the Type 1 PCTF should be replaced by the confocal PCTF. The procedure for generating the confocal PCTF has been described in detail in sec. 6.1. The procedure for increasing the resolution of the output signal in the Type 1 reflectance scanning microscope, described in sec 6.2.1 can be applied in the single detector MO system.

Impulse response

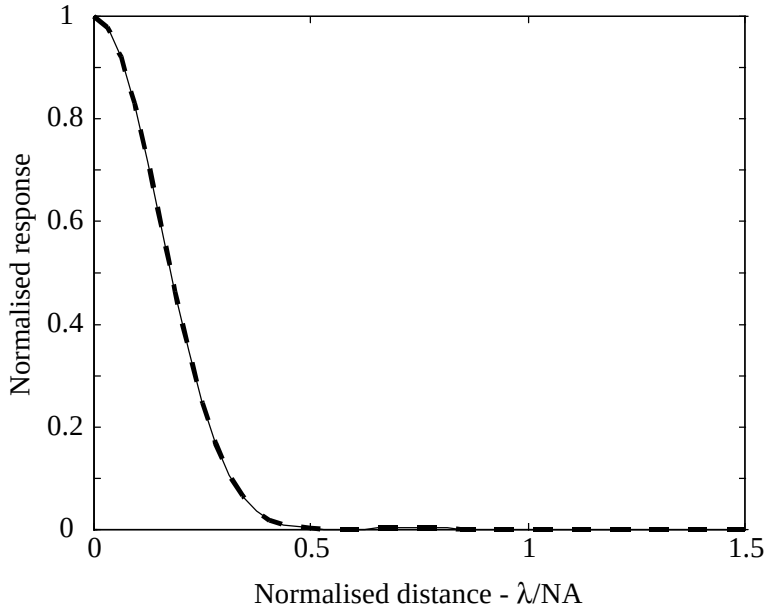

Figure 6.14 : *The impulse response of the ideal confocal single detector MO scanning microscope (solid line). Also illustrated is the impulse response of the Type 1 reflectance system (bold dashed line).*

Figure 6.14 illustrates the impulse response of the ideal confocal single detector MO system, i.e. an infinitesimally small pinhole, generated using the transfer function algorithm with clear, aberration free, circular apertures of equal diameter under uniform incident illumination, for an analyser orientation of β=90° to the angle of incident polarisation. Also illustrated is the impulse response of the confocal reflectance system under the same conditions.

Figure 6.14 illustrates that as in the Type 1 configuration, the impulse response of the confocal single detector MO scanning microscope is identical to that of the confocal reflectance scanning microscope offering similar improved resolution characteristics, for an analyser set to extinction.

6.3.3 Analyser misalignment in the MO single detector scanning microscope

If it is assumed that the MO sample is of uniform reflectance, such that $\Gamma(n_x) = d(n_x)$ and $\Gamma^*(n_x') = d(n_x')$, then the medium function for the single detector MO scanning microscope, eq. (4.15), reduces to the form

$$M(n_x;n_x') = \left(d(n_x')\cos b + \Lambda^*(n_x')\sin b\right)\left(d(n_x)\cos b + \Lambda(n_x)\sin b\right) \quad (6.9)$$

which by substituting into eq. (6.4) and rearranging gives

$$\begin{aligned} I(x_s) = \iint_{-\infty}^{\infty} C(n_x;n_x')\Big(& d(n_x)d(n_x')\cos^2 b + d(n_x)\Lambda^*(n_x')\sin b \\ & + d(n_x')\Lambda(n_x)\sin b + \Lambda(n_x)\Lambda^*(n_x')\sin^2 b \Big) \\ & \cdot \exp\{2pj(n_x x_s - n_x' x_s')\}\; dn_x\; dn_x' \Big|_{x_s'=x_x} \end{aligned} \quad (6.10)$$

which by further simplification gives

$$\begin{aligned} I(x_s) = {} & C(0;0)\cos^2 b + \int_{-\infty}^{\infty} C(0;n_x')\Lambda^*(n_x')\sin b\, dn_x' \\ & + \int_{-\infty}^{\infty} C(n_x;0)\Lambda(n_x)\sin b\, dn_x + \iint_{-\infty}^{\infty} C(n_x;n_x')\Lambda(n_x)\Lambda^*(n_x')\sin^2 b\, dn_x\; dn_x' \end{aligned} \quad . \quad (6.11)$$

It can be seen from eq. (6.11) that for analyser orientation of $b°$ to the plane of the incident polarisation, the signal for the photo-detector comprises a dc term, which is a

function of the PCTF at the origin, terms which depend upon the product of the axial values of the PCTF and the spectra of the MO information, and a term which depends upon the product of the PCTF and the spectra of the MO information over all $(n_x;n_x')$ space. Thus, it can be seen that for any analyser misalignment from the extinction position, $b = 90°$, the signal will contain an undesirable dc offset. If the analyser is aligned so as to minimise the dc offset, i.e. $b = 90°$, then the signal from the photo-detector reduces to the form

$$I(x_s, y_s) = \int_{-\infty}^{\infty} C(0;n_x')\Lambda^*(n_x')dn_x' + \int_{-\infty}^{\infty} C(n_x;0)\Lambda(n_x)dn_x + \iint_{-\infty}^{\infty} C(n_x;n_x')\Lambda(n_x)\Lambda^*(n_x')dn_x\ dn_x' \quad . \qquad (6.12)$$

The dc term in eq. (6.11) arises due to the propagation of the *x*-component of polarisation, which contains no MO information, through the analyser when it is aligned away from the optimum position. As the angle of the misalignment increases then more of the *x*-component, and less of the *y*-component containing the MO information, propagates through the analyser and contributes to an increased dc level from the photo-detector. Figure 6.15 illustrates the dc offset and the magnitude of the impulse response of the signal from the single detector MO system, as a function of analyser orientation (in degrees). The responses were generated using the transfer function approach with clear, aberration free, circular apertures of equal diameter under uniform illumination. The MO sample was of uniform reflectance (equal to unity) and zero phase. The plot of dc level has been normalised to the maximum value, which is observed when $b = 0°$, and the plot of the magnitude of the impulse response has been normalised to the maximum value, which is observed when $b = 45°$. It should be noted that for an analyser orientation above $b = 90°$ the impulse response is in fact a negative pulse superimposed on the positive dc level.

Figure 6.15 clearly illustrates that misalignment of the analyser transmission axis introduces an extremely large dc level into the signal from the photo-detector. Even though the maximum magnitude of the impulse response occurs at $b = \pm 45°$, not at the optimum position, $b = 90°$. However, at $b = \pm 45°$ the signal is swamped by a

large dc level. Hence, it can be seen that the orientation of the analyser transmission axis needs to be aligned so as to maximise the Kerr signal obtained from the photo-detector and remove the dc level. It should be noted that a similar trend is observed in the confocal mode of operation.

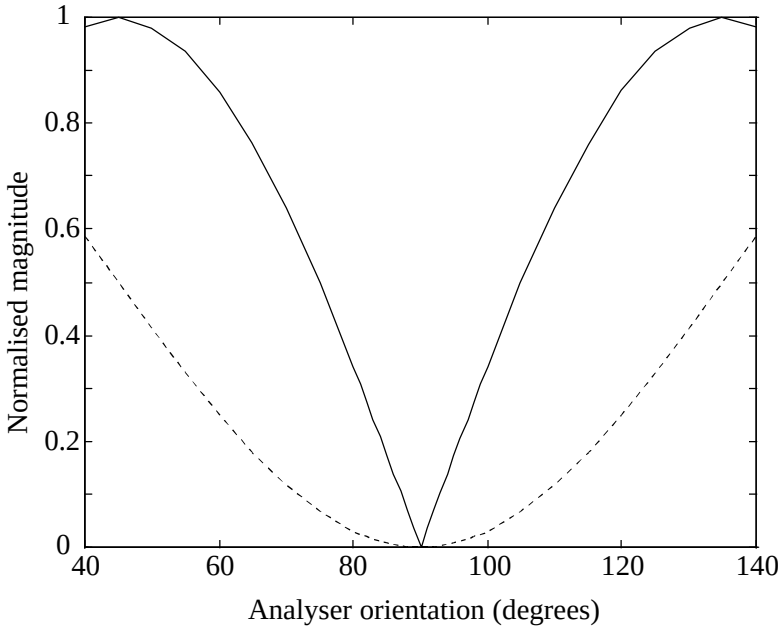

Figure 6.15 : *Plot of dc offset (dashed line) and the magnitude of the impulse response (solid line) of the signal from the Type 1 single detector MO system, as a function of analyser alignment, for a MO sample of uniform reflectance and zero phase.*

It has been previously mentioned that typically the analyser is aligned at 8° to the extinction position. This can be seen to increase the magnitude of the response whilst at the same time introducing very little dc offset.

6.4 Modelling the differential detector MO scanning microscope

In this section the imaging process in the differential detector MO scanning microscope is discussed, using the transfer function approach. The signal from the differential detector MO scanning microscope can be expressed in the characteristic form of eq. (3.32), where the PCTF depends upon whether the detection channel is Type 1 or confocal, and the medium function is given by eq. (4.42). Considering

objects which contain information in a single direction only, x, then the medium function may be recast in the simplified form

$$\begin{aligned} M(n_x;n_x') = &\left(\Gamma(n_x)\Gamma^*(n_x') - \Lambda(n_x)\Lambda^*(n_x')\right)\cos 4q \\ &+\left(\Gamma(n_x)\Lambda^*(n_x) + \Gamma^*(n_x')\Lambda(n_x)\right)\sin 4q \end{aligned} \tag{6.13}$$

and the characteristic equation, eq. (3.32), can be expressed in the form of eq. (6.4).

The following analysis will be directed to calculating the form of the readout signal for both the Type 1 and confocal differential configurations, when imaging simple one-dimensional objects.

6.4.1 The Type 1 system

The computational procedure for calculating the response from the Type 1 differential detector MO scanning microscope follows directly from the procedure described in sec. 6.3.1. However, the medium function in the differential detector MO scanning microscope, eq. (6.13), is different to that of the single detector MO scanning microscope and so the computational procedure for calculating the response differs slightly from that illustrated in sec. 6.3.1.

The transfer function algorithm

The algorithm illustrated below, written in pseudocode (see Appendix B), for generating the response from the Type 1 differential detector MO scanning microscope to a simple one-dimensional MO object, is modified from the algorithm presented in sec. 6.3.1.

Step 1 Input data.

Matrix containing the objective aperture pupil function - p_o, of dimensions $adim \times adim$
Matrix containing the collector aperture pupil function - p_c, of dimensions $adim \times adim$
Vector containing the sample reflectance characteristics - r, of length *mdim* (one-dimensional MO object)
Vector containing the sample phase characteristics - f, of length *mdim* (one-dimensional MO object)
Vector containing the sample Kerr rotation characteristics - k, of

length *mdim* (one-dimensional MO object)
The angle of the half wave plate fast axis - *q*.
Matrix to contain the PCTF - *P*, of dimensions *mdim* × *mdim*.
Matrix to contain the medium function - *M*, of dimensions *mdim* × *mdim*.
Vector to contain the MO spectrum of the object - Λ, of length *mdim*.
Vector to contain the reflectance spectrum of the object - Γ, of length *mdim*.
Temporary vectors - *dummy* and *temp*, of length *mdim*.

Output data. Vector containing the signal from the scanning microscope - *I*, of length *mdim*.

Step 2 Generate a matrix representing the Type 1 PCTF, *PCTF*, using the algorithm presented in sec. 6.1, which is of dimensions *tdim* × *tdim*, where *tdim* = 2×*adim*.

Step 3
FOR *y = 1…mdim*
  FOR *x = 1…mdim*
    Set *P*(*y*, *x*) = 0;
  END;
END;
FOR *y = 1…tdim*
  FOR *x = 1…tdim*
    Set *P*(*y* + ((*mdim*-*tdim*)/*2*), *x* + ((*mdim*-*tdim*)/*2*)) = *PCTF*(*y*, *x*);[#1]
  END;
END.

Step 4 Set Γ = Fast Fourier Transform (*r*); [#2]
Set Λ = Fast Fourier Transform (*r* .× *f* .× *tan*(*k*)). [#3]

Step 5
FOR *x = 1…mdim*
  Set ℜ (Γ*(*x*)) = ℜ (Γ(*x*)); [#4]
  Set ℑ (Γ*(*x*)) = - ℑ (Γ(*x*));
END;
FOR *x = 1…mdim*
  Set ℜ (Λ*(*x*)) = ℜ (Λ(*x*)); [#4]
  Set ℑ (Λ*(*x*)) = - ℑ (Λ(*x*));
END.

Step 6
FOR *y = 1…mdim*
  FOR *x = 1…mdim*
    Set *M*(*y*, *x*) = (Γ(*x*)× Γ*(*y*)-Λ(*x*) × Λ*(*y*))*cos4q*
      +(Γ(*x*)× Λ*(*y*)+Λ(*x*) × Γ*(*y*))*sin4q*;
  END;
END.

Step 7
FOR *y = 1…mdim*
  FOR *x = 1…mdim*
    Set *P*(*y*, *x*) = *P*(*y*, *x*) × *M*(*y*, *x*);
  END;

END.

Step 8 FOR *y = 1…mdim*
FOR *x = 1…mdim*
Set *dummy*(*x*) = *P*(*y*, *x*);
END;
Set *dummy* = Fast Fourier Transform (*dummy*); [#5]
FOR *x = 1…mdim*
Set *temp*(*y*, *x*) = *P*(*x*);
END;
END.

Step 9 FOR *y = 1…mdim*
FOR *x = 1…mdim*
Set *dummy*(*x*) = *P*(*x*, *y*);
END;
Set *dummy* = Inverse Fast Fourier Transform (*dummy*); [#4]
FOR *x = 1…mdim*
Set *P*(*x*, *y*) = *dummy*(*x*);
END;
END.

Step 10 FOR *x = 1…mdim*
Set *I* (*x*) = *P*(*x*, *x*);
END;
STOP.

[#1] Centre the PCTF inside the larger *temp* matrix of dimensions *mdim* × *mdim*.
[#2] Fast Fourier Transform algorithm is described in reference 6.
[#3] .× indicates array multiplication.
[#4] $\Re$ - represents the real component, $\Im$ - represents the imaginary component.
[#5] Inverse Fast Fourier Transform algorithm is described in reference 6.

Step response

For an object with information in a single direction only, *x*, and a half wave plate orientation of $q = 22.5°$, the medium function, eq. (6.13), simplifies to give

$$M(n_x; n_x') = \left(\Gamma(n_x)\Lambda^*(n_x') + \Gamma^*(n_x')\Lambda(n_x)\right). \tag{6.14}$$

Assuming the MO sample has uniform ordinary reflectance, such that $r_x(x_o) = 1$ and hence $\Gamma(n_x) = d(n_x)$, substituting into the eq. (6.4) allows the signal from the Type 1 differential detector MO system to be expressed in the form

$$I(x_s) = \int_{-\infty}^{\infty} C(0; n_x')\Lambda^*(n_x')\exp\{-2pj(n_x' x_s)\}dn_x' + \int_{-\infty}^{\infty} C(n_x; 0)\Lambda(n_x)\exp\{2pj(n_x x_s)\}dn_x \tag{6.15}$$

and it can be seen that the signal is now a function of the MO sample spectrum, $\Lambda(n_x)$, and the form of the Type 1 PCTF, $C(n_x;n_x')$, along the $n_x = 0$ and $n_x' = 0$ axes.

The signal generation process in the Type 1 differential detector MO system is subtly different from that of the reflectance and single detector MO scanning microscopes where generally the signal depends on the form of the PCTF over all $(n_x;n_x')$ space. Thus, in the case of an optimally aligned half wave plate, and a sample of uniform reflectance (r_x), the response of the differential detection MO case can be calculated by straightforward Fourier transforms of the product of the MO object spectra and the axial values of the Type 1 PCTF.

Figure 6.16 illustrates the step response of the Type 1 differential detector MO scanning microscope, generated using the transfer function algorithm, with the half wave plate fast axis aligned at 22.5°.

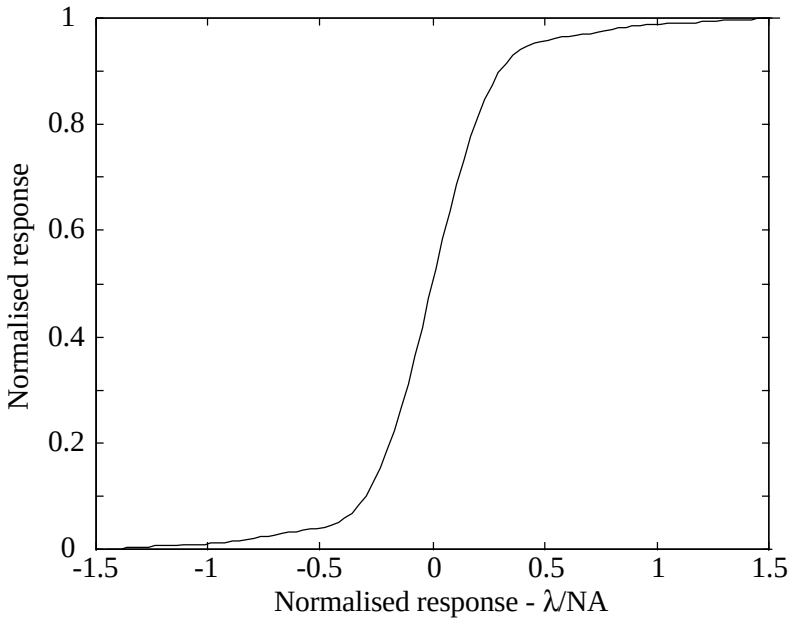

Figure 6.16 : *The step response of the Type 1 differential detector MO system for clear, aberration free, circular apertures of equal diameter under uniform incident illumination, generated using the transfer function approach.*

Comparison of Fig. 6.16 with Fig. 5.14 illustrates that the two approaches to modelling the imaging process in the Type 1 differential detector MO scanning microscope, the direct calculation and transfer function approaches, produce exactly the same results when imaging simple one-dimensional objects.

Impulse response

Consider the impulse response of a MO sample of uniform reflectance (r_x equal to unity), and an impulse in the tangent of Kerr rotation, i.e. $\tan(a(x_o)) = d(x_o)$. The sample MO spectrum is uniform, i.e. $\Lambda(n_x) = \Lambda^*(n_x') = 1$, and the signal from the Type 1 differential detector MO system is given by

$$I(x_s) = \int_{-\infty}^{\infty} C(0;n_x')\exp\{-2pj(n_x' x_s)\}dn_x' + \int_{-\infty}^{\infty} C(n_x;0)\exp\{2pj(n_x x_s)\}dn_x \quad (6.16)$$

and the signal is determined by the one-dimensional Fourier transform of the axial values of the Type 1 PCTF.

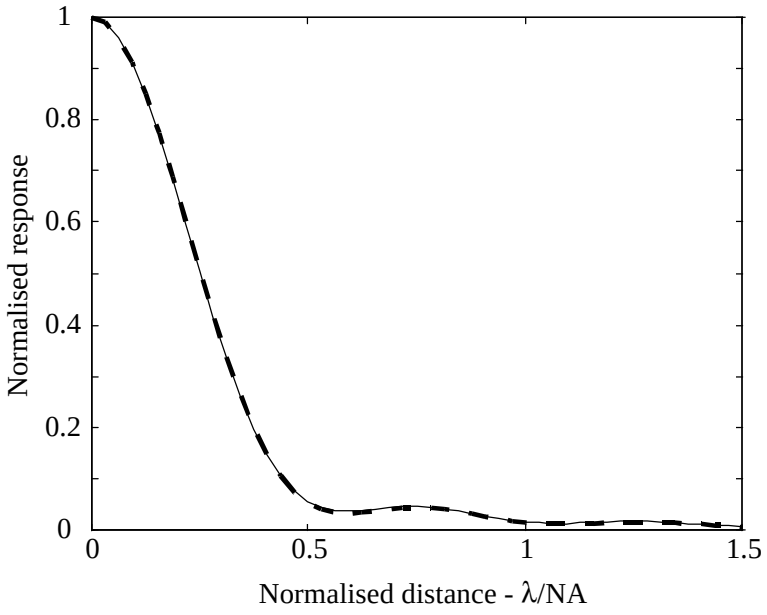

Figure 6.17 : *The impulse response of the Type 1 differential detector MO. Also illustrated is the impulse response of the incoherent optical system (bold dashed line).*

The resulting response for the differential detector MO scanning microscope, generated using the transfer function algorithm, with the half wave plate fast axis

aligned at 22.5° is shown in Fig. 6.17. This is identical to that of the incoherent optical system described in sec. 3.1.2. This is to be expected since the axial form of the PCTF has the same functional form described by the relationship of eq. (3.26).

6.4.2 The confocal system

The computational procedure, using the transfer function approach, for calculating the response of the confocal differential detector MO scanning microscope follows directly from the algorithm described in detail in sec. 6.4.1. However, when calculating the response of the confocal configuration, the Type 1 PCTF should be replaced by the confocal PCTF. The computational procedure for generating the confocal PCTF has been described in detail in sec. 6.1.

Impulse response

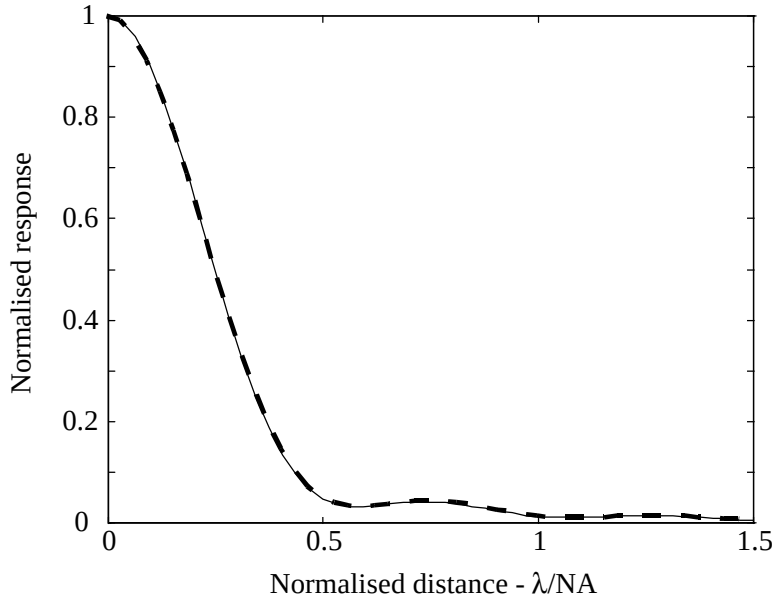

Figure 6.18 : *Plot of the impulse response of the differential detector MO system for the ideal confocal configuration (solid line), the Type 1 configuration (bold dashed line), for clear, aberration free, circular apertures under uniform illumination.*

Figure 6.18 illustrates the impulse response of the confocal differential detector MO scanning microscope, employing an infinitesimally small pinhole with the half wave

plate fast axis aligned at 22.5°, generated using the transfer function algorithm. The response was generated using clear, aberration free, circular apertures of equal diameter, under uniform incident illumination, using a MO sample of uniform reflectance (r_x equal to unity) and zero phase. Also illustrated is the impulse response of the Type 1 configuration under the same conditions.

It can be clearly seen that the response of the ideal confocal differential detector MO system is identical to that of the Type 1 system described previously. This interesting and perhaps surprising result indicates that, unlike the confocal reflectance system and the single detector MO system, the confocal differential detector MO system offers no improved lateral resolution over the Type 1 configuration. This has important consequences for the design of MO SLMs, a point that will be discussed in more detail later.

It was shown previously that for an MO sample of uniform ordinary reflectance, the signal from the differential detector MO system is found by taking the Fourier transform along the axial values of the PCTF, whether the configuration is Type 1 or confocal. However, it can be shown that the axial variation of the PCTF is identical in both the Type 1 and ideal confocal cases, and that they are in fact identical to the axial values of the incoherent OTF illustrated in Fig. 3.6. Figure 6.19 illustrates the form of the incoherent OTF, the Type 1 PCTF and the ideal confocal PCTF along the $n_x = 0$ axis, for clear, aberration free, circular apertures of equal diameter under uniform illumination. It can be clearly seen that the axial values of the three transfer functions are identical.

Hence, it has been shown that the confocal differential detector MO system, offers no improved lateral resolution over the Type 1 configuration, and that both systems have imaging characteristics identical to that of the incoherent reflectance imaging system, assuming the MO sample is of uniform ordinary reflectance (r_x equal to unity).

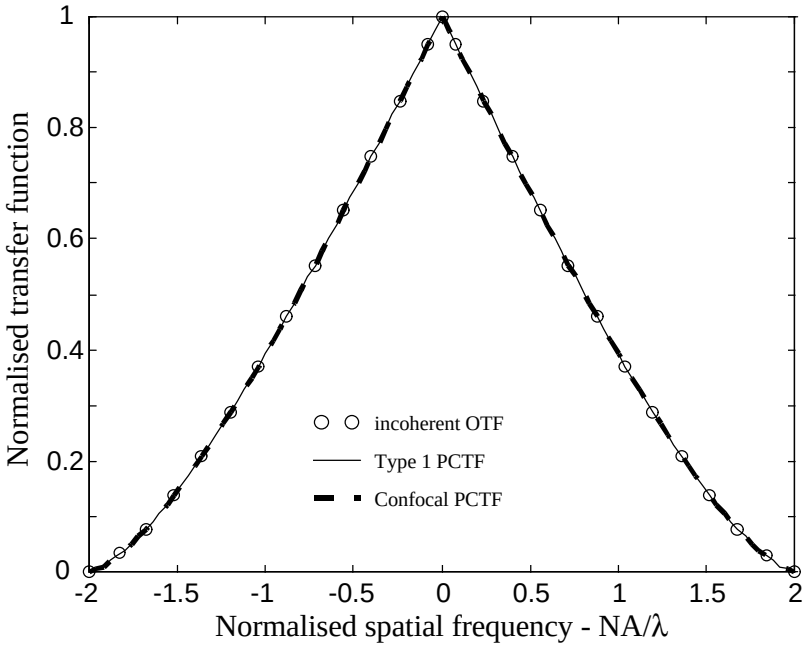

Figure 6.19 : *Plot along the $n_x = 0$ axis of the incoherent OTF, the Type 1 PCTF and the ideal confocal PCTF, for clear, aberration free, circular apertures of equal diameter under uniform illumination.*

6.4.3 Pinhole size and resolution issues in the confocal differential detector MO scanning microscope

It is illustrated in Fig. 6.18 that the impulse response of the confocal differential detector MO scanning microscope employing an infinitesimally small pinhole, is identical to that of the Type 1 configuration, when the MO sample if of uniform reflectance. However, it is instructive to investigate the effects which the size of the confocal pinhole has upon the response of the confocal differential detector MO system. Figure 6.20 illustrates a plot of FWHM of the impulse response of the confocal differential detector MO system as a function of pinhole radius. The responses were generated using the transfer function approach with clear, aberration free, circular apertures of equal diameter, under uniform incident illumination. The MO sample was of uniform reflectance (r_x equal to unity) and zero phase. The plot has been normalised with respect to the FWHM of the impulse response of the Type 1 differential detector MO system under the same conditions. Also illustrated, for

comparison purposes, is a plot of FWHM against pinhole radius of the impulse response of the confocal reflectance system, under the same conditions.

Figure 6.20 illustrates that the size of the confocal pinhole has very little effect on the FWHM of the impulse response of the differential detector MO scanning microscope. In fact, the resolution for a truly infinitesimally small pinhole is identical to that for no confocal pinhole at all (Type 1 case). In fact a pinhole size of around 0.7λ/NA leads to a slight degradation in resolution performance. This result is somewhat surprising and has certainly not featured in any of the published literature to date. It has important implications for the design of MO scanning laser microscopes and will discussed further in chapter 9.

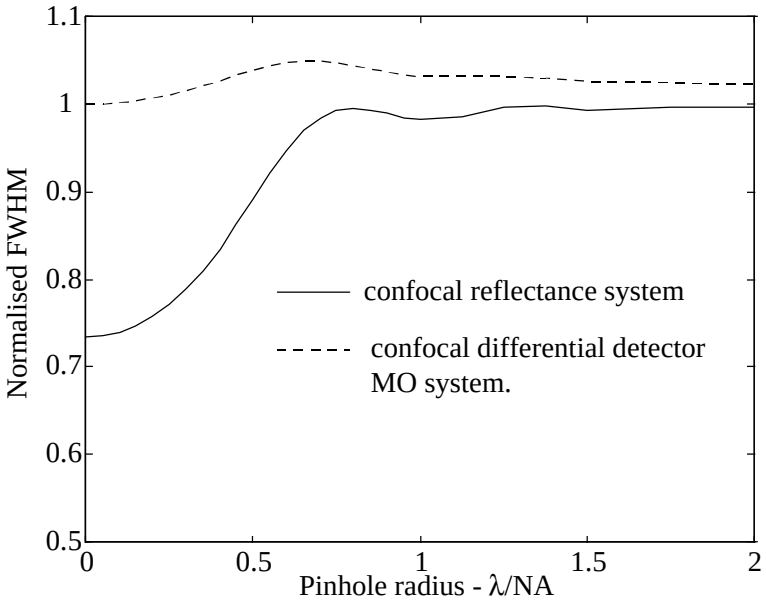

Figure 6.20 : *Plot of FWHM of the impulse response of the confocal differential detector MO system as a function of pinhole size, for a MO sample of uniform reflectance and zero phase.*

6.4.4 Half wave-plate misalignment in the differential detector MO scanning microscope

It was illustrated in sec. 6.4.1 that if the MO sample is of uniform reflectance and zero phase, and the fast axis of the half wave plate is aligned at 22.5° to the angle of the

incident plane of polarisation, then the response of the differential detector MO system depends upon the axial values of the PCTF. However, what effect would misalignment of the half wave plate from the optimum position have upon the response of the differential detector MO scanning microscope?

Expressing the signal from the differential detector MO system in terms of the reflectance and MO properties of the sample gives

$$I(x_s) = \iint_{-\infty}^{\infty} C(n_x;n_x')\Big\{\big(\Gamma(n_x)\,\Gamma^*(n_x') - \Lambda(n_x)\Lambda^*(n_x')\big)\cos 4q + \big(\Gamma(n_x)\,\Lambda^*(n_x') + \Gamma^*(n_x')\Lambda(n_x)\big)\sin 4q\Big\}dn_x\,dn_x' \tag{6.17}$$

which if we assume the MO sample is of uniform reflectance, i.e. $\Gamma(n_x) = d(n_x)$ and $\Gamma^*(n_x') = d(n_x')$, can be expressed in the form

$$I(x_s) = C(0;0)\cos 4q - \iint_{-\infty}^{\infty} C(n_x;n_x')\Lambda(n_x)\Lambda^*(n_x')\cos 4q\,dn_x\,dn_x' + \int_{-\infty}^{\infty} C(0;n_x')\Lambda^*(n_x')\sin 4q\,dn_x' + \int_{-\infty}^{\infty} C(n_x;0)\Lambda(n_x)\sin 4q\,dn_x \tag{6.18}$$

and when $q = 22.5°$ the signal will depend upon the axial values of the PCTF, as shown previously. However, misalignment of the half wave plate introduces two extra terms into the response of the differential detector MO system. The first of these is a constant dc term governed by the angle of misalignment and the value of the PCTF at the origin, and the second depends upon the form of the PCTF over all $(n_x;n_x')$ space.

Figure 6.21 illustrates plots of dc level and the magnitude of the impulse response of the differential detector MO scanning microscope, as a function of half wave plate orientation (in degrees). The responses were generated using the transfer function approach, with clear, aberration free, circular apertures of equal diameter, under uniform incident illumination. The MO sample was of uniform reflectance (r_x equal to unity) and zero phase. The impulse response magnitude has been normalised with respect to the maximum value, which occurs when $q = 22.5°$, and the dc level magnitude has been normalised with respect to the maximum value, which occurs when $q = 0°$.

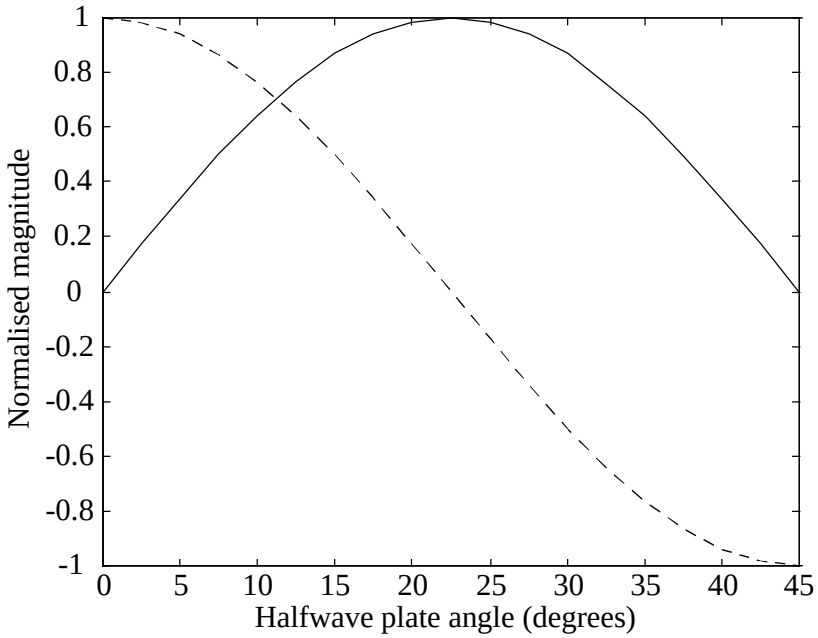

Figure 6.21 : *Plot of the dc level (dashed line) and magnitude of the impulse response (solid line) of the differential detector MO system, for a MO sample of uniform reflectance and zero phase.*

Figure 6.21 illustrates that when the fast axis of the half wave plate is aligned at its optimum value, $q = 22.5°$, the dc level will be removed and the magnitude of the impulse response will be at its maximum. However, misalignment of the half wave plate reduces the magnitude of the impulse response whilst at the same introducing a large dc offset into the observed signal. It should be noted that the FWHM of the impulse response remains unaffected by the rotation of the half wave plate. Apart from the orientation $q = 0°$ where MO contrast is no longer observed. It should be noted that a similar trend is observed in the confocal mode of operation.